EIF4A3-Mediated CircRNA_100290 Promotes GC Cell Proliferation, Invasion and EMT via miR-29b-3p/ITGA11 Axis

Gang Wang
First Affiliated Hospital of china Medical University https://orcid.org/0000-0001-9318-6251
Dan Sun
First Affiliated Hospital of China Medical University
Wenhui Li
First affiliated hospital of china medical university
Yan Xin (yxin@cmu.edu.cn)
Fisrst Affiliated Hospital of China Medical University https://orcid.org/0000-0002-8809-5803

Research

Keywords: circRNA_100290, miR-29b-3p/ITGA11 axis, EIF4A3, EMT, gastric cancer

Posted Date: May 17th, 2020

DOI: https://doi.org/10.21203/rs.3.rs-28082/v1

Abstract

Background Circular RNA (circRNA) has been reported as an important regulator in the development and progression of various carcinomas. However, the role of circRNA_100290 in gastric cancer (GC) is still unclear. This study aimed to investigate the role of circRNA_100290 in GC invasion and metastasis and its possible mechanism.

Methods The expression of circRNA_100290 in GC cells and tissues were examined using quantitative real-time polymerase chain reaction (qRT-PCR). The role of circRNA_100290 in cell proliferation, migration, and invasion was evaluated on AGS and HGC-27 cell lines *in vitro*. Bioinformatics tools, dual-luciferase reporter assay, Western blot assay and qRT-PCR were used to explore the downstream pathways of circRNA_100290. The mechanism underlying the regulation of the expression of circRNA_100290 was explored using RNA immunoprecipitation, qRT-PCR, and Western blot assays.

Results The expression of circRNA_100290 was found significantly upregulated in GC cells and 102 GC tissues, high expression of circRNA_100290 in GC was closely related to Borrmann's types, lymph node metastasis and tumor-node-metastasis staging. In vitro, knockdown of circRNA_100290 in AGS and HGC-27 cells significantly inhibited cell proliferation, migration, and invasion. Mechanistically, dual-luciferase reporter assay confirmed a direct binding between circRNA_100290 and miR-29b-3p, which targets *ITGA11*, an oncogene which is closely related to epithelial–mesenchymal transition (EMT). In addition, EIF4A3, one of RNA binding proteins (RBPs), could inhibit the formation of circRNA_100290 via enriching flanking sites of circRNA_100290. Low expression of EIF4A3 in GC was related to a worse prognosis.

Conclusions Elevated circRNA_100290 in GC promotes cell proliferation, invasion and EMT via miR-29b-3p/ITGA11 axi and might be regulated by EIF4A3. CircRNA_100290 might be a promising biomarker and target for GC therapy.

Background

Gastric cancer (GC) is the fifth most frequently diagnosed malignancy and the third leading cause of cancer death worldwide[1]. According to Chinese cancer statistics, in 2014, the new cases of GC in China were approximately 410,000 and the deaths were approximately 294,000, which was second only to lung cancer[2]. Although abundant advances have been made in diagnostics and new therapeutic approaches of GC, a large number of patients with GC end up with poor prognosis. Therefore, appropriate molecular biomarkers of early diagnosis and potential treatment targets for GC need to be developed.

CircRNAs are a unique category of RNA molecules formed via back-splicing. They have neither 5'–3' polarities nor polyadenylated tails, which were first identified in plant viruses in the 1970s and now exist widely in eukaryotes[3,4]. Recently, various circRNAs have been found to participate in tumorigenesis and progression[5,6]. CircRNAs are suitable biomarkers of diseases usually because they own covalently closed-loop structures, are more stable than corresponding linear RNAs, and are insusceptible to the

degradation of RNase R. In addition, circRNAs often exhibit specific expression in various diseases and tissues[4,7,8]. More convincing evidence demonstrated that circRNAs were dysregulated in GC. CircRNA_001569 and circPDSS1 were reported to be overexpressed in GC and accelerated GC progression by sponging miR-145 and miR-186-5p, respectively[9,10]. Circ_0027599/PHDLA1, circLARP4, and circPVRL3 functioned as tumor suppressors and inhibited the growth and metastasis of GC cells[11–13]. Previous studies reported that circRNA_100290 was upregulated and functioned as a miRNA sponge in oral squamous cell carcinoma and colorectal cancer[14,15]. However, the role of circRNA_100290 in GC is still unclear. In addition, splicing factors and RNA-binding proteins (RBPs) might regulate the formation of circRNAs via back-splicing[16,17], but the regulatory mechanism of circRNA_100290 in GC is still unknown.

The present study was novel in demonstrating that circRNA_100290 was overexpressed in GC samples and cell lines. *In vitro*, silencing the expression of circRNA_100290 suppressed GC cell proliferation, induced G0/G1 phase arrest, and impeded migration, invasion, and EMT via miR-29b-3p/ITGA11 axis. The present study provides a promising biomarker and an effective target for GC treatment.

Materials And Methods

Clinical specimen collection

A total of 102 fresh GC and matched normal gastric epithelial tissues were acquired from patients with GC undergoing resection in The First Affiliated Hospital of China Medical University. All the clinical-pathological data was classified according to the Eighth Edition of AJCC Clinical Practice Guidelines for GC. This study was approved by the ethics committee of The First Affiliated Hospital of China Medical University, and informed consent was obtained from patients.

Cell culture and transfection

GC cell lines AGS, BGC-823, SGC-7901, and HGC-27 and human immortalized normal gastric epithelial cells GES-1 were provided and identified by Genechem Co., Ltd (Shanghai, China). Hsa_circ_100290 and EIF4A3 siRNA and paired negative control sequence were designed and synthesized by GenePharma (China). The si-CircRNA_100290 sequence of sense strand was 5'-CUCAUGCUUAGGCUUGAUUdTdT-3'; the sequence of the antisense strand was 3'-dTdTGAGUACGAAUCCGAACUAA-5'. The si-EIF4A3 sequence of sense strand was 5'-CGAGCAAUCAAGCAGAUCAdTdT-3', and the sequence of the antisense strand was 3'-dTdTGCUCGUUAGUUCGUCUAGUdTdT-5'. AGS and HGC-27 cells were prepared for si-circRNA_100290 and si-EIF4A3 transfection using Lipofectamine reagent (GenePharma, China) according to the manufacturer's protocol. The knockdown efficiency was detected by quantitative real-time polymerase chain reaction (qRT-PCR) assay 48 h after transfection.

RNA extraction and real-time PCR

RNA was extracted from GC cells and tissues using miRcute miRNA Kits (Tiangen Biotech Co., Ltd, Beijing, China) following the instructions. The concentration and quality of RNA was evaluated using

NanoDrop spectrophotometer (Thermo Scientific, USA). Then, extracted RNA underwent reverse transcription using PrimeScript Master Mix (TaKaRa, Japan) and MiR-X miRNA First-Strand Synthesis Kit (Takara, Japan) for mRNA and miRNA according to the manual instructions, respectively. The primers were constructed and synthesized by Sangon Biotech (Shanghai, China). The qRT-PCR assay was performed, and the expression levels were calculated using the $2^{-\triangle\triangle Ct}$ method. Glyceraldehyde-3-phosphate dehydrogenase (GAPDH) was used as the internal reference for circRNA_100290 and mRNA expression detection, and U6 was used as the internal reference for detection of miR-29b-39 expression. The reaction conditions were as follows: 95 °C for 30 s; 40 cycles of 95 °C for 5 s, annealing at 56 °C for 32 s; dissolving curve at 95 °C for 15 s, 60 °C for 30 s, and 95 °C for 15 s. The primers for were as follows: circRNA_100290 forward: 5'-CACGGACACAGTCATTCCCT-3' and reverse: 5'-ATCAAGCCTAAGCATGAGAATGAAA-3'; miR-29b-3p forward: 5'-TAGCACCATTTGAAATCAGTGTT-3'; ITGA11 forward: 5'-GGAGGAAGACTTGCGTCG-3' and reverse: 5'-CACAGGTTCCCCAGTAGATG-3'. EIF4A3 forward: 5'-CGCGGACTCTGACATATGGCGACCACGGCCACGATG-3' and reverse: 5'-TCCCGCAGGCCCATGGTGTCG-3'; GAPDH forward: 5'-GAGTCAACGGATTTGGTCGT-3' and reverse: 5'-TTGATTTTGGAGGGATCTCG-3'; U6: forward: 5'- GGAACGATACAGAGAAGATTAGC-3' and reverse: 5'-TGGAACGCTTCACGAATTTGCG-3'.

Plasmid transfection and luciferase assays

Luciferase reporter gene plasmid containing the 3'-UTR region or mutated 3'-UTR region of circRNA_100290 and miR-29-3p overexpression plasmid were constructed by GeneChem Co., Ltd (Shanghai, China). Then, 20 ng reporter construct and 80 ng miRNA expression plasmid, along with 4 ng Renilla luciferase plasmid, were co-transfected into H293T cells in a 96-well plate using jetPRIME transfection reagent (PolyPlus, France) as described by the manufacturer. The transfection efficiency was evaluated by fluorescence microscopy. The luciferase activity was measured 48-h after transfection using the dual-luciferase reporter assay system as described by the manufacturer (Promega, USA).

Western blot

Western blot assay was conducted followed by previous report[18]. Concentration of primary antibody: anti-EIF4A3 (1:1000, Abcam, USA), anti-E-cadherin (1:1000, CST, USA), anti-Vimintin(1:1000, CST, USA), anti-N-cadherin (1:1000, CST, USA) and GAPDH (1:1000, Origene Co., Ltd., Beijing, China).

RNA immunoprecipitation assay

The RNA-Binding Protein Immunoprecipitation (Millipore, USA) was used to perform a RIP assay. According to the manufacturer's protocol, 1×10^7 cells were harvested and lysed in complete RIPA lysis buffer. RNA magnetic beads were conjugated to anti-EIF4A3 (Abcam, USA) or control anti-IgG (Millipore, USA). The Ct value of circRNA_100290 was detected by qRT-PCR.

Colony formation assay

Two hundred GC cells were seeded in six-well plates and incubated for 11 days. After being washed, fixed, and stained with 0.01% crystal violet, the cell clones were imaged and evaluated using Quantity One

software.

Cell counting kit (CCK-8) assay

Two thousand GC cells were plated in 96-well plates. 10 μl CCK-8 (Solarbio, Beijing, China) reagent were seeded and incubated for 3 h at 37 °C atmosphere. Then, the absorbance at 450 nm was detected and recorded for five consecutive days.

Flow cytometry analysis for cell cycle

The cell fixation was conducted using 70% ethanol for 24 h. Then, the cells were stained using PI and RNase reagent and incubated for 30 min at 37 °C. The cell cycle distribution analysis was performed using flow cytometry device (BD, USA).

Wound healing assay

About 3×10^5 cells were plated into a 6-well dish. A linear scratch was made using a sterile 10-μL pipette tip when the cell convergence degree reached 90%. The cell scratch wound was washed with PBS and treated with RPMI1640 supplemented with 3% fetal bovine serum. The cell scratch wound was imaged under a microscope after 0, 24, and 48 h. Then, the wound healing rate was analyzed using ImageJ software.

Transwell migration and invasion assay

Transwell inserts (Corning, USA) were used to perform cell migration and invasion assays. The membrane was not coated with Matrigel (BD, USA) for cell migration assay. GC cells were added into the upper chamber and cultured in an incubator at 37 °C for 24 h. Then migrated cells were fixed, stained with crystal violet and recorded. For the cell invasion assay, the membrane was coated with Matrigel and serum-free medium mixture (BD, USA), and the culture was incubated at 37 °C for 48 h.

Bioinformatics analysis

Bioinformatics prediction was performed using *RNA22 v2.0*, *Starbase* and *Circintera ctome* [19–21]. The array data of miRNAs and mRNAs were obtained from The European Bioinformatics Institute (EBI), Gene Expression Omnibus (GEO) and The Cancer Genome Atlas (TCGA)[22–24]. The function protein association of ITGA11 was analyzed using *STRING* [25].The survival curve was plotted using R software and *Kaplan–Meier plotter* [26].

Statistical analysis

GraphPad Prism 8.0.2 and SPSS 25.0 software was used for statistical analysis. Data were presented as mean ± standard error of the mean. The χ2 test, Student t test, and one-way analysis of variance were used for comparisons. Pearson correlation coefficient was calculated to measure correlation between factors. TA P value less than 0.05 was considered statistically significant.

Results

Expression of CircRNA_100290 was upregulated in GC tissues

qRT-PCR was performed to examine the expression of circRNA_100290 in 102 paired GC tissues. The results showed that the expression of circRNA_100290 in GC was significantly higher than that in paired adjacent noncancerous tissues (Fig. 1A). Moreover, analysis of clinicopathological characteristics revealed that the expression of circRNA_100290 in GC tissues was closely related to Borrmann's types, lymph node metastasis and TNM stage (Table 1).

Table 1
Relevance analysis between expression of circRNA_100290 and clinicopathological characteristics in Chinese patients with GC

Characteristics	N = 102	Expression of circRNA_100290		χ2	*P*
		Low	High		
Gender				0.475	0.491
Male	74	42	32(43.2%)		
Female	28	18	10 (35.7%)		
Age(years)				0.545	0.460
≤ 60	37	20	17(45.9%)		
> 60	65	40	25(38.5%)		
Borrmann's types				4.092	**0.043**
I + II	13	11	2(15.4%)		
III	89	49	40(44.9%)		
WHO's histological types				1.849	0.604
Tubular Ade.					
Moderately Diff.	29	18	11(37.9%)		
Poorly Diff.	63	35	28(44.4%)		
Mucinous Ade.	8	5	3(37.5%)		
Signet ring cell car.	2	2	0(0.00%)		
Lauren's types				1.199	0.549
Intestinal	22	15	7(31.8%)		
Diffuse	70	40	30(42.9%)		
Mixed	10	5	5(50.0%)		
Tumor diameter(cm)				0.038	0.846
≤ 4.5	40	24	16(40.0%)		
> 4.5	62	36	26(41.9%)		
Depth of invasion				0.467	0.495

Ade. Adenocarcinoma; Diff. Differentiated; Car. Carcinoma; Ln. Lymph node

[a]Fisher's exact test

Characteristics	N = 102	Expression of circRNA_100290		χ2	*P*
		Low	High		
T2 + T3	33	21	12(36.4%)		
T4	69	39	30(43.5%)		
Ln metastasis				10.336	**0.006**
N0	24	20	4(16.7%)		
N1 + N2	42	25	17(40.5%)		
N3	36	15	21(58.3%)		
Distant metastasis					1.000[a]
M0	98	58	40 (40.8%)		
M1	4	2	2 (50.0%)		
TNM Staging				5.446	**0.020**
I + II	27	21	6(22.2%)		
III + IV	75	39	36(48.0%)		
Ade. Adenocarcinoma; Diff. Differentiated; Car. Carcinoma; Ln. Lymph node					
[a]Fisher's exact test					

Expression of miR-29b-3p decreased in GC and could be sponged by CircRNA_100290

CircRNAs customarily function as miRNA sponges to bind functional miRNAs. Hence, *RNA22 V2.0* was used to predict miRNAs having potential binding sites with circRNA_100290 (Fig. 1B). Then, miR-29b-3p was chosen for further research. The qRT-PCR assay was conducted to examine the expression of miR-29b-3p in 31 matched GC tissues. The results showed a diminished expression of miR-29b-3p in GC tissues (Fig. 1C). Subsequently, the expression of miR-29b-3p in GC was validated by analyzing data downloaded from the EBI database which contained 184 GC tissues and 168 normal gastric epitheliums, and a same expression trend was observed (Fig. 1D). The correlation analysis results demonstrated a negative correlation between the expression of circRNA_100290 and miR-29b-3p in GC tissues ($r = -0.3656$, $P = 0.047$; Fig. 1E). Additionally, luciferase reporter plasmids were transfected into H293T cells to further explore the relationship between circRNA_100290 and miR-29b-3p. The dual-luciferase reporter assay revealed that miR-29b-3p mimics reduced the luciferase activity in the wild-type group, indicating miR-29b-3p as a target for circRNA_100290 (Fig. 1F&G).These data suggested that miR-29b-3p might act as a tumor suppressor and circRNA_100290 could serve as a molecular sponge for miR-29b-3p in GC.

Expression of ITGA11 increased in GC and negatively correlated with the expression of miR-29b-3p in GC tissues

Starbase was used to predict the possible target genes of miR-29b-3p. *ITGA11*, one potential target gene, might have binding sites in 3'-UTR with miR-29b-3p (Fig. 2A). The expression and function of *ITGA11* in GC were not completely clear. qRT-PCR was conducted to examine the expression of *ITGA11* in 31 GC tissues. The results showed that the expression level of *ITGA11* in GC tissues was higher than that in paired noncancerous tissues (Fig. 2B). Data were downloaded from the TCGA database to further explore the role ITGA11 plays in GC. Clinicopathological characteristic analysis showed *ITGA11* expression was closely related to Lauren's types, invasion depth and TNM stage (Table 2). Furthermore, the correlation analysis showed a negative correlation between the expression of miR-29b-3p and *ITGA11* in GC ($r = -0.3168$, $P = 0.009$; Fig. 2C).

Table 2
Relevance analysis between expression of ITGA11 and clinicopathological characteristics in GC patients from TCGA database

Characteristics	N	Expression of ITGA11		χ2	*P*
		Low	High		
Gender	375			2.161	0.142
Male	241	114	127(52.7%)		
Female	134	74	60(44.8%)		
Age(years)	371			0.61	0.435
< 65	155	81	74(47.7%)		
≥ 65	216	104	112(51.9%)		
Histological grade	366			1.921	0.166
G1 + G2	147	80	67(45.6%)		
G3	219	103	116(53.0%)		
Lauren's types[a]	229			7.323	**0.026**
Intestinal	157	77	80(51.0%)		
Diffuse	55	18	37(67.3%)		
Mixed	17	4	13(76.5)		
Depth of invasion	367			22.669	**0.000**
T1	19	18	1 (5.30%)		
T2	80	46	34(42.5%)		
T3	168	85	83(49.4%)		
T4	100	38	62(62.0%)		
Ln metastasis	357			5.471	0.14
N0	111	64	47(42.3%)		
N1	97	52	45(46.4%)		
N2	75	33	42(56.0%)		
N3	74	32	42(56.8%)		

[a] Lauren's types data of 146 GC cases is unavailable.

Ln. Lymph node

Characteristics	N	Expression of ITGA11		χ2	*P*
		Low	High		
Distant metastasis	355			1.169	0.28
M0	330	169	161(48.8%)		
M1	25	10	15(60.0%)		
TNM Staging	352			13.737	**0.003**
I	53	39	14(26.4%)		
II	111	54	57(51.4%)		
III	150	69	81(54.0%)		
IV	38	16	22(57.9%)		
[a] Lauren's types data of 146 GC cases is unavailable.					
Ln. Lymph node					

Subsequently, the prognostic value of the expression of *ITGA11* in 354 GC patients from the TCGA database was evaluated. *ITGA11* high-expression group displayed a lower 5-year survival rates (Fig. 2D). High expression of *ITGA11* predicted poor prognosis in GC. In addition, the protein–protein interaction (PPI) analysis on ITGA11 was conducted using the STRING software. Potential proteins interacting with ITGA11 included integrin family members, collagen family members, transforming growth factor family members, and so on. Gene ontology (GO) analysis revealed that the aforementioned proteins were mainly involved in migration-related biological processes, such as extracellular matrix organization, cell adhesion and migration, and so on (Fig. 2E).

CircRNA_100290 promoted proliferation, colony formation, and cell cycle distribution of GC via miR-29b-3p/ITGA11 axis

The expression levels of circRNA_100290 and miR-29b-3p were assessed in four GC cell lines and GES-1. The expression of circRNA_100290 was upregulated in AGS, BGC-823, and HGC-27 compared with GES-1, while miR-29b-3p was downregulated correspondingly (Fig. 3A&B). AGS and HGC-27 cell lines were chosen for further knocking down of circRNA_100290 as a higher circRNA_100290 expression. After knocking down circRNA_100290, the expression of miR-29b-3p and *ITGA11* presented increasing and decreasing trends, respectively in both cells (Fig. 3C&D).

The CCK8 assay was performed to compare the cell viability of GC. For five consecutive days, the absorbance value in si-circRNA_100290 AGS and HGC-27 cells was found to be obviously lower compared with that in the control groups, indicating that knocking down circRNA_100290 inhibited GC

cell proliferation (Fig. 3E&F). The results of cell colony formation assay demonstrated that the colony numbers in si-circRNA_100290 AGS and HGC-27 cells were less than those in control groups (Fig. 3G-3J). Reduced circRNA_100290 suppressed the colony formation ability of GC cells. The cell cycle distribution was detected by flow cytometry. Decreased circRNA_100290 induced the increased percentage of the G0/G1 phase and downregulated the ratio of S and G2/M phases in si-circRNA_100290 AGS and HGC-27 cells (Fig. 3K-3N). The results suggested that knocking down circRNA_100290 might induce G0/G1 arrest and inhibit GC cell proliferation

CircRNA_100290 accelerated GC cell migration and invasion through regulating EMT

The cell wound healing and Transwell migration assays were performed to measure the effect of circRNA_100290 on cell migration and invasion abilities. Cell wound healing assay demonstrated that the wound healing rate was significantly lower in si-circRNA_100290 AGS and HGC-27 groups compared with the control groups (Fig. 4A). The statistical diagrams of AGS and HGC-27 groups showed that the most significant difference between the experimental and control groups was observed after 48 h (Fig. 4B&C). Transwell migration assay showed that the impaired migration ability was observed in si-circRNA_100290 AGS and HGC-27 cells. The number of GC cells migrating into the lower chamber was less in si-circRNA_100290 groups compared with the control (Fig. 4D-4G). The results of Transwell invasion assay also revealed that the reduced expression of circRNA_100290 damaged the cell invasion ability. The number of AGS and HGC-27 cells invading into the lower chamber remarkably reduced after knocking down circRNA_100290 (Fig. 4H-4K). Moreover, Western Blot assay demonstrated that knocking down of circRNA_100290 induced the increased E-cadherin and reduced expression of N-cadherin and Vimentin (Fig. 4L).

EIF4A3 could bind flanking region of circRNA_100290 and inhibited circRNA_100290 expression in GC

To find out the molecular mechanism underlying the regulation of the expression of circRNA_100290, Circinteractome, one of the bioinformatics tools, was used to predict circRNA_100290 related RBPs. EIF4A3 had the most potential binding sites matched with circRNA_100290 and its flanking regions compared with other RBPs (Fig. 5A). Therefore, EIF4A3 was chosen for further study. RIP assay was performed to determine the binding between EIF4A3 and flanking regions of circRNA_100290 in AGS and HGC-27 cells. The RIP-qPCR results showed 8.18- and 4.31-fold enrichment of the flanking site of circRNA_100290 in AGS and HGC-27 cells, respectively (Fig. 5B). In addition, after the knocking down of EIF4A3, an increased level of circRNA_100290 was observed in both cells (Fig. 5C).

Expression of EIF4A3 was decreased in GC, and low-expressed EIF4A3 predicted poor prognosis of patients with GC

qRT-PCR and Western blot assays were performed to assess the expression of EIF4A3 in 31 matched GC tissues. The results showed that the expression of EIF4A3 at both mRNA and protein levels was significantly downregulated in GC (Fig. 5D&E). Besides, the prognostic value of the expression of EIF4A3 in 876 patients with GC from the GEO database was evaluated by using the Kaplan–Meier plotter website. The results showed that the low expression of EIF4A3 was associated with worse overall survival (OS) and first progression (FP). The median OS in the low–EIF4A3 expression group was 26.27 months, shorter than that in the high–EIF4A3 expression group (30.9 months). Comparably, the median FP in the low–EIF4A3 expression group was 14.1 months shorter than that in the high–EIF4A3 expression group (21.73 months) (Fig. 5F&G**)**. Subsequently, clinicopathological analysis was conducted to explore the role EIF4A3 plays in GC by using datasets GSE62254[27] containing 300 GC patients from GEO database. Results revealed that the expression of EIF4A3 in GC was closely related to sex, age, Lauren's type, invasion depth, TNM staging, and ACRG genotyping (Table 3). The data above suggested that EIF4A3 might serve as a suppressor in GC, and reduced expression of EIF4A3 predicted worse prognosis of patients with GC.

Table 3
Relevance analysis between expression of EIF4A3 and clinicopathological characteristics in GC patients from GEO database[a]

Characteristics	N = 300	Expression of EIF4A3		χ2	*P*
		Low	High		
Gender				5.513	**0.019**
Male	199	20(10.1%)	179		
Female	101	20(19.8%)	81		
Age(years)				7.887	**0.005**
≤ 63	148	28(18.9%)	120		
> 63	152	12(7.9%)	140		
Lauren's types				22.73	**0.000**
Intestinal	146	7(4.8%)	139		
Diffuse	134	32(23.9%)	102		
Mixed	17	1(5.9%)	16		
Depth of invasion				8.897	**0.012**
T2	188	17(9%)	171		
T3	91	20(22%)	71		
T4	21	3(14.3%)	18		
Ln metastasis				1.114	0.291
N0	38	3(7.9%)	35		
N1 ~ N3	262	37(15.3%)	225		
Distant Metastasis				0.902	0.342
M0	273	38(13.9%)	235		
M1	27	2(7.4%)	25		
TNM Staging				8.916	**0.030**
I	31	1(3.2%)	30		

[a]GEO accession number: GSE62254

Ln. Lymph node; ACRG Asian Cancer Research Group; mol. molecular; MSI microsatellite instability; MSS Microsatellite stability; $TP53^-$ TP53 inactive; $TP53^+$ TP53 active; EMT epithelial-to-mesenchymal transition

Characteristics	N = 300	Expression of EIF4A3		χ2	*P*
		Low	High		
II	97	12(12.4%)	85		
III	95	20(21.1%)	75		
IV	77	7(9.1%)	70		
ACRG's mol. types				34.989	**0.000**
MSI	68	1(1.5%)	67		
MSS/TP53$^-$	107	8(7.5%)	99		
MSS/TP53$^+$	79	14(17.7%)	65		
MSS/EMT	46	17(37%)	29		
[a]GEO accession number: GSE62254					
Ln. Lymph node; ACRG Asian Cancer Research Group; mol. molecular; MSI microsatellite instability; MSS Microsatellite stability; TP53$^-$ TP53 inactive; TP53$^+$ TP53 active; EMT epithelial-to-mesenchymal transition					

Discussion

CircRNAs, a new class of noncoding RNAs (ncRNAs), has gradually gained attention. It has been reported that exonic-originated circRNAs located mainly in the cytoplasm usually function as miRNA 'sponges'[6]. CircRNAs also participate in transcriptional or post-transcriptional regulation[28,29]. Moreover, several circRNAs containing internal ribosome entry sites could be translated into peptides[30]. However, the acknowledged circRNAs and their regulatory mechanism in GC have not been thoroughly elaborated. CircRNA_100290, one of circRNAs discovered recently, is located on chromosome 1, and its parental gene is *SLC30A7*. A recent study reported that circRNA_100290 was abnormally highly expressed in colorectal cancer and promoted the proliferation of colorectal cells[15]. In the present study, circRNA_100290 was significantly upregulated in GC, and was closely related to invasion depth, lymph node metastasis, and TNM stage. Functionally, silencing circRNA_100290 in AGS and HGC-27 cells significantly inhibited cell viability, colony formation, migration, and invasion ability, and induced the G0/G1 phase arrest *in vitro*. These results suggested that circRNA_100290 might serve as an oncogene in GC.

CircRNAs might function as miRNA sponges via binding miRNAs and regulate downstream target genes, also known as competing endogenous RNA regulatory mechanism. In our study, the expression of miR-29b-3p was found to be decreased in GC and this trend was validated by analyzing data from the EBI database. MiR-29b-3p is a member of miR-29 family, decreased expression of miR-29 family members has been reported in various tumors, including lung cancer, esophageal cancer, hepatocellular carcinoma,

and so on[31–33]. The bioinformatic prediction and correlation analysis indicated miR-29b-3p might share the complementary binding sites with circRNA_100290, which was confirmed by the dual-luciferase reporter assay, suggesting that circRNA_100290 could function as a sponge for miR-29b-3p. Taken together, our results suggested that miR-29b-3p acted as a tumor suppressor and interacted with circRNA_100290 by sponging in GC.

ITGA11, a candidate target of miR-29b-3p, was further studied. *ITGA11* is a member of the integrin family. It is unregulated in various tumors, such as lung cancer, breast cancer, meningeal glioma and so on[34–36]. However, the role of *ITGA11* in GC has not been reported so far. The present study reported an elevated expression of *ITGA11* in GC, which was reversed to the expression of miR-29b-3p. Pathological factors analysis and survival analysis indicated that high expression of *ITGA11* predicted a worse prognosis of GC patients. *ITGA11* might serve as an oncogene in GC. Furthermore, silencing circRNA_100290 in AGS and HGC-27 cells led to the increased miR-29b-3p and diminished *ITGA11*, suggesting circRNA_100290 could sponge miR-29b-3p to increase the expression of *ITGA11*, thereby promoting GC cell proliferation, migration and invasion.

Growing evidence demonstrates that circRNAs usually regulate tumor progression and metastasis by affecting EMT[37,38]. In our study, knocking down of circRNA_100290 induced altered expression of several EMT markers, accompanied by the release of miR-29b-3p and blocking of ITGA11. Previous studies have reported the involvement of miR-29b family members in EMT[39]. In addition, there is report reveals that miR-29b could inhibit EMT and metastasis by targeting a network of pro-metastatic motivators involved in angiogenesis, collagen remodeling, and proteolysis[40]. Shin et al. reported that exogenous miR-29b mediated an anticancer effect by impeding the activation of *ITGA11*[36]. In our study, by using PPI and GO analyses, ITGA11 was found to have a close connection with EMT-related proteins and could be involved in EMT. These results reflected that circRNA_100290 promoted EMT mainly via the miR-29b-3p/ITGA11 axis.

CircRNAs are formatted via back-splicing regulated by RNA splicing factors or RBPs[41,42]. In this study, EIF4A3 was found to have the most predicted binding sites among other RBPs with both flanking regions and circRNA_100290 itself, and RIP assay confirmed the direct interaction between flanking regions of circRNA_100290 and EIF4A3. As a member of the DEAD-box protein family, EIF4A3 is located mainly in the nucleus, and is a part of the exon junction complex necessary for nonsense-mediated mRNA decay[43]. In addition, EIF4A3 is also involved in various biological processes, including mRNA translation initiation and RNA splicing[44,45]. It was inferred that EIF4A3 was probably involved in the transcriptional regulation of circRNA_100290. Wang et al. reported that EIF4A3 could induce circMMP9 cyclization and increased expression of circMMP9 in GBM by binding to the MMP9 mRNA transcript[46]. Inconsistent with that, we found silenced *EIF4A3* led to the elevated circRNA_100290, indicated that EIF4A3 could inhibit the formation of circRNA_100290. The regulatory mechanisms of circRNAs was complicated. Inverted Alu repeats could promote circRNA formation by facilitating back-splicing of pre-mRNAs, while DHX9, an RBP, bound specifically to inverted-repeat Alu elements, thereby inhibiting the formation of circRNAs. The loss

of DHX9 led to an increase in the number of circular RNAs[47]. In addition, Ivanov et al. reported that ADAR1 could decrease the expression of circRNA by competitively binding with reverse complementary sequences highly enriched in introns bracketing circRNAs[48]. EIF4A3 might inhibit the formation of circRNA_100290 by binding the flanking regions of circRNA_100290.These studies suggested that the role of EIF4A3 in different circRNAs' cyclization is distinct, the underlying mechanism remains further explore.

Additionally, we found the expression of EIF4A3 was down regulated in GC. Moreover, low expression of EIF4A3 was found to predict a worse prognosis and was closely related to Lauren's type, invasion depth, and TNM staging by analyzing pathological factors in GSE62254, a dataset from the GEO database, which contained 300 GC cases. By comprehensive sequencing, 300 GC cases were classified into four subtypes, including MSI, MSS/EMT, MSS/TP53^{+} and MSS/TP53^{-}, according to the ACRG molecular type[49]. Interestingly, EIF4A3 high-expression group had the lowest percentage of MSS/EMT subtype of ACRG genotyping. Previous study reported that GC patients with MSS/EMT subtype had the worst OS and the highest rate of recurrence, especially involving peritoneal dissemination[50]. The results indicated that EIF4A3 functioned as a tumor suppressor and negative regulator of circRNA_100290 in GC.

Conclusions

In conclusion, our study reveals that the expression of circRNA_100290 was upregulated in GC. Further, the knockdown of circRNA_100290 significantly inhibited GC cell proliferation, migration, and invasion *in vitro*. The potential mechanism could be that circRNA_100290 regulated EMT via targeting miR-29b-3p/ITGA11. In addition, EIF4A3 could serve as a negative regulator of circRNA_100290 and a tumor suppressor in GC. CircRNA_100290might serve as a potential biomarker and an effective target for GC diagnosis and therapy.

Abbreviations

GC
Gastric cancer; CircRNA:Circular RNA; qRT-PCR:quantitative real-time polymerase chain reaction; miRNA:microRNA; MRE:miRNA response element; EMT:Epithelial-mesenchymal transition; RBP:RNA-binding protein; RIP:RNA Immunoprecipitation; OS:Overall survival; FP:First progression; ACRG:Asian Cancer Research Group.

Declarations

Ethics approval and consent to participate

The studies involving human participants were reviewed and approved by the ethics committee of The First Affiliated Hospital of China Medical University. The patients/participants provided their written

informed consent to participate in this study.

Consent for publication

Not applicable.

Availability of data and materials

The data that support the findings of this study are available from the corresponding author upon reasonable request.

Competing interests

The authors declare that they have no competing interests.

Funding

This study was supported by the National Natural Science Foundation of China (No.81971584, No.81071650); Special foundation for Science and Technology Program in Liaoning Province, China (2013225585); and Supporting Project for Climbing Scholars in Liaoning Provincial Universities, China (2009).

Authors' contributions

GW and DS were responsible for performing the experiments and drafted the manuscript. GW and Wh L were responsible for acquisition and analysis of data. GW and DS provided and collected the clinical data. YX were responsible for designing the experiments and supervising the study. All authors read and approved the final manuscript.

Acknowledgements

Not applicable.

References

1. Bray F, Ferlay J, Soerjomataram I, Siegel RL, Torre LA, Jemal A. Global cancer statistics 2018: GLOBOCAN estimates of incidence and mortality worldwide for 36 cancers in 185 countries. CA Cancer J Clin. 2018;68(6):394–424.
2. Chen W, Sun K, Zheng R, Zeng H, Zhang S, Xia C, Yang Z, Li H, Zou X, He J. Cancer incidence and mortality in China, 2014. Chin J Cancer Res. 2018;30(1):1–12.

3. Sanger HL, Klotz G, Riesner D, Gross HJ, Kleinschmidt AK. Viroids are single-stranded covalently closed circular RNA molecules existing as highly base-paired rod-like structures. Proc Natl Acad Sci U S A. 1976;73(11):3852–6.
4. Salzman J, Gawad C, Wang PL, Lacayo N, Brown PO. Circular RNAs are the predominant transcript isoform from hundreds of human genes in diverse cell types. PLoS One. 2012;7(2):e30733.
5. Qu S, Yang X, Li X, Wang J, Gao Y, Shang R, Sun W, Dou K, Li H. Circular RNA. A new star of noncoding RNAs. Cancer Lett. 2015;365(2):141–8.
6. Chen Y, Li C, Tan C, Liu X. Circular RNAs: a new frontier in the study of human diseases. J Med Genet. 2016;53(6):359–65.
7. Memczak S, Jens M, Elefsinioti A, Torti F, Krueger J, Rybak A, Maier L, Mackowiak SD, Gregersen LH. Munschauer M and others. Circular RNAs are a large class of animal RNAs with regulatory potency. Nature. 2013;495(7441):333–8.
8. Jeck WR, Sorrentino JA, Wang K, Slevin MK, Burd CE, Liu J, Marzluff WF, Sharpless NE. Circular RNAs are abundant, conserved, and associated with ALU repeats. RNA. 2013;19(2):141–57.
9. Shen F, Liu P, Xu Z, Li N, Yi Z, Tie X, Zhang Y, Gao L. CircRNA_001569 promotes cell proliferation through absorbing miR-145 in gastric cancer. J Biochem. 2019;165(1):27–36.
10. Ouyang Y, Li Y, Huang Y, Li X, Zhu Y, Long Y, Wang Y, Guo X, Gong K. CircRNA circPDSS1 promotes the gastric cancer progression by sponging miR-186-5p and modulating NEK2. J Cell Physiol. 2019;234(7):10458–69.
11. Wang L, Shen J, Jiang Y. Circ_0027599/PHDLA1 suppresses gastric cancer progression by sponging miR-101-3p. 1. Cell Biosci. 2018;8:58.
12. Zhang J, Liu H, Hou L, Wang G, Zhang R, Huang Y, Chen X, Zhu J. Circular RNA_LARP4 inhibits cell proliferation and invasion of gastric cancer by sponging miR-424-5p and regulating LATS1 expression. Mol Cancer. 2017;16(1):151.
13. Sun HD, Xu ZP, Sun ZQ, Zhu B, Wang Q, Zhou J, Jin H, Zhao A, Tang WW, Cao XF. Down-regulation of circPVRL3 promotes the proliferation and migration of gastric cancer cells. Sci Rep. 2018;8(1):10111.
14. Chen X, Yu J, Tian H, Shan Z, Liu W, Pan Z, Ren J. Circle RNA hsa_circRNA_100290 serves as a ceRNA for miR-378a to regulate oral squamous cell carcinoma cells growth via Glucose transporter-1 (GLUT1) and glycolysis. J Cell Physiol. 2019;234(11):19130–40.
15. Fang G, Ye BL, Hu BR, Ruan XJ, Shi YX. CircRNA_100290 promotes colorectal cancer progression through miR-516b-induced downregulation of FZD4 expression and Wnt/beta-catenin signaling. Biochem Biophys Res Commun. 2018;504(1):184–9.
16. Ashwal-Fluss R, Meyer M, Pamudurti NR, Ivanov A, Bartok O, Hanan M, Evantal N, Memczak S, Rajewsky N, Kadener S. circRNA biogenesis competes with pre-mRNA splicing. Mol Cell. 2014;56(1):55–66.
17. Petkovic S, Muller S. RNA circularization strategies in vivo and in vitro. Nucleic Acids Res. 2015;43(4):2454–65.

18. Sun D, Li X, He Y, Li W, Wang Y, Wang H, Jiang S, Xin Y. YAP1 enhances cell proliferation, migration, and invasion of gastric cancer in vitro and in vivo. Oncotarget. 2016;7(49):81062–76.
19. Miranda KC, Huynh T, Tay Y, Ang YS, Tam WL, Thomson AM, Lim B, Rigoutsos I. A pattern-based method for the identification of MicroRNA binding sites and their corresponding heteroduplexes. Cell. 2006;126(6):1203–17.
20. Li JH, Liu S, Zhou H, Qu LH, Yang JH. starBase v2.0: decoding miRNA-ceRNA, miRNA-ncRNA and protein-RNA interaction networks from large-scale CLIP-Seq data. Nucleic Acids Res. 2014;42(Database issue):D92-7.
21. Dudekula DB, Panda AC, Grammatikakis I, De S, Abdelmohsen K, Gorospe M. CircInteractome. A web tool for exploring circular RNAs and their interacting proteins and microRNAs. RNA Biol. 2016;13(1):34–42.
22. Rodriguez-Tome P, Stoehr PJ, Cameron GN, Flores TP. The European Bioinformatics Institute (EBI) databases. Nucleic Acids Res. 1996;24(1):6–12.
23. Barrett T, Wilhite SE, Ledoux P, Evangelista C, Kim IF, Tomashevsky M, Marshall KA, Phillippy KH, Sherman PM. Holko M and others. NCBI GEO: archive for functional genomics data sets–update. Nucleic Acids Res. 2013;41(Database issue):D991-5.
24. Tomczak K, Czerwinska P, Wiznerowicz M. The Cancer Genome Atlas (TCGA): an immeasurable source of knowledge. Contemp Oncol (Pozn). 2015;19(1A):A68–77.
25. Szklarczyk D, Gable AL, Lyon D, Junge A, Wyder S, Huerta-Cepas J, Simonovic M, Doncheva NT, Morris JH. Bork P and others. STRING v11: protein-protein association networks with increased coverage, supporting functional discovery in genome-wide experimental datasets. Nucleic Acids Res. 2019;47(D1):D607–13.
26. Lanczky A, Nagy A, Bottai G, Munkacsy G, Szabo A, Santarpia L, Gyorffy B. miRpower: a web-tool to validate survival-associated miRNAs utilizing expression data from 2178 breast cancer patients. Breast Cancer Res Treat. 2016;160(3):439–46.
27. Cristescu R, Lee J, Nebozhyn M, Kim KM, Ting JC, Wong SS, Liu J, Yue YG, Wang J, Yu K. and others. Molecular analysis of gastric cancer identifies subtypes associated with distinct clinical outcomes. Nat Med. 2015;21(5):449–56.
28. Tay Y, Rinn J, Pandolfi PP. The multilayered complexity of ceRNA crosstalk and competition. Nature. 2014;505(7483):344–52.
29. Li Z, Huang C, Bao C, Chen L, Lin M, Wang X, Zhong G, Yu B, Hu W. Dai L and others. Exon-intron circular RNAs regulate transcription in the nucleus. Nat Struct Mol Biol. 2015;22(3):256–64.
30. Salzman J. Circular RNA, Expression. Its Potential Regulation and Function. Trends Genet. 2016;32(5):309–16.
31. Yanaihara N, Caplen N, Bowman E, Seike M, Kumamoto K, Yi M, Stephens RM, Okamoto A, Yokota J. Tanaka T and others. Unique microRNA molecular profiles in lung cancer diagnosis and prognosis. Cancer Cell. 2006;9(3):189–98.

32. Ding DP, Chen ZL, Zhao XH, Wang JW, Sun J, Wang Z, Tan FW, Tan XG, Li BZ, Zhou F and others. miR-29c induces cell cycle arrest in esophageal squamous cell carcinoma by modulating cyclin E expression. Carcinogenesis 2011;32(7):1025-32.
33. Xiong Y, Fang JH, Yun JP, Yang J, Zhang Y, Jia WH, Zhuang SM. Effects of microRNA-29 on apoptosis, tumorigenicity, and prognosis of hepatocellular carcinoma. Hepatology. 2010;51(3):836–45.
34. Chong IW, Chang MY, Chang HC, Yu YP, Sheu CC, Tsai JR, Hung JY, Chou SH, Tsai MS, Hwang JJ. and others. Great potential of a panel of multiple hMTH1, SPD, ITGA11 and COL11A1 markers for diagnosis of patients with non-small cell lung cancer. Oncol Rep. 2006;16(5):981–8.
35. Duss S, Brinkhaus H, Britschgi A, Cabuy E, Frey DM, Schaefer DJ, Bentires-Alj M. Mesenchymal precursor cells maintain the differentiation and proliferation potentials of breast epithelial cells. Breast Cancer Res. 2014;16(3):R60.
36. Shin J, Shim HG, Hwang T, Kim H, Kang SH, Dho YS, Park SH, Kim SJ, Park CK. Restoration of miR-29b exerts anti-cancer effects on glioblastoma. Cancer Cell Int. 2017;17:104.
37. Wang T, Wang X, Du Q, Wu N, Liu X, Chen Y, Wang X. The circRNA circP4HB promotes NSCLC aggressiveness and metastasis by sponging miR-133a-5p. Biochem Biophys Res Commun. 2019;513(4):904–11.
38. Zhang X, Luo P, Jing W, Zhou H, Liang C, Tu J. circSMAD2 inhibits the epithelial-mesenchymal transition by targeting miR-629 in hepatocellular carcinoma. Onco Targets Ther. 2018;11:2853–63.
39. Chou J, Lin JH, Brenot A, Kim JW, Provot S, Werb Z. GATA3 suppresses metastasis and modulates the tumour microenvironment by regulating microRNA-29b expression. Nat Cell Biol. 2013;15(2):201–13.
40. Melo SA, Kalluri R. miR-29b moulds the tumour microenvironment to repress metastasis. Nat Cell Biol. 2013;15(2):139–40.
41. Meng J, Chen S, Han JX, Qian B, Wang XR, Zhong WL, Qin Y, Zhang H, Gao WF. Lei YY and others. Twist1 Regulates Vimentin through Cul2 Circular RNA to Promote EMT in Hepatocellular Carcinoma. Cancer Res. 2018;78(15):4150–62.
42. Dai X, Zhang N, Cheng Y, Yang T, Chen Y, Liu Z, Wang Z, Yang C, Jiang Y. RNA-binding Protein Trinucleotide repeat-containing 6A Regulates the Formation of Circular RNA 0006916, with Important Functions in Lung Cancer Cells. Carcinogenesis 2018.
43. Gehring NH, Kunz JB, Neu-Yilik G, Breit S, Viegas MH, Hentze MW, Kulozik AE. Exon-junction complex components specify distinct routes of nonsense-mediated mRNA decay with differential cofactor requirements. Mol Cell. 2005;20(1):65–75.
44. Holzmann K, Gerner C, Poltl A, Schafer R, Obrist P, Ensinger C, Grimm R, Sauermann G. A human common nuclear matrix protein homologous to eukaryotic translation initiation factor 4A. Biochem Biophys Res Commun. 2000;267(1):339–44.
45. Zhang Z, Krainer AR. Splicing remodels messenger ribonucleoprotein architecture via eIF4A3-dependent and -independent recruitment of exon junction complex components. Proc Natl Acad Sci

U S A. 2007;104(28):11574–9.

46. Wang R, Zhang S, Chen X, Li N, Li J, Jia R, Pan Y, Liang H. EIF4A3-induced circular RNA MMP9 (circMMP9) acts as a sponge of miR-124 and promotes glioblastoma multiforme cell tumorigenesis. Mol Cancer. 2018;17(1):166.
47. Aktas T, Avsar Ilik I, Maticzka D, Bhardwaj V, Pessoa Rodrigues C, Mittler G, Manke T, Backofen R, Akhtar A. DHX9 suppresses RNA processing defects originating from the Alu invasion of the human genome. Nature. 2017;544(7648):115–9.
48. Ivanov A, Memczak S, Wyler E, Torti F, Porath HT, Orejuela MR, Piechotta M, Levanon EY, Landthaler M. Dieterich C and others. Analysis of intron sequences reveals hallmarks of circular RNA biogenesis in animals. Cell Rep. 2015;10(2):170–7.
49. Ye XS, Yu C, Aggarwal A, Reinhard C. Genomic alterations and molecular subtypes of gastric cancers in Asians. Chin J Cancer. 2016;35:42.
50. Katona BW, Rustgi AK. Gastric Cancer Genomics: Advances and Future Directions. Cell Mol Gastroenterol Hepatol. 2017;3(2):211–7.

Figures

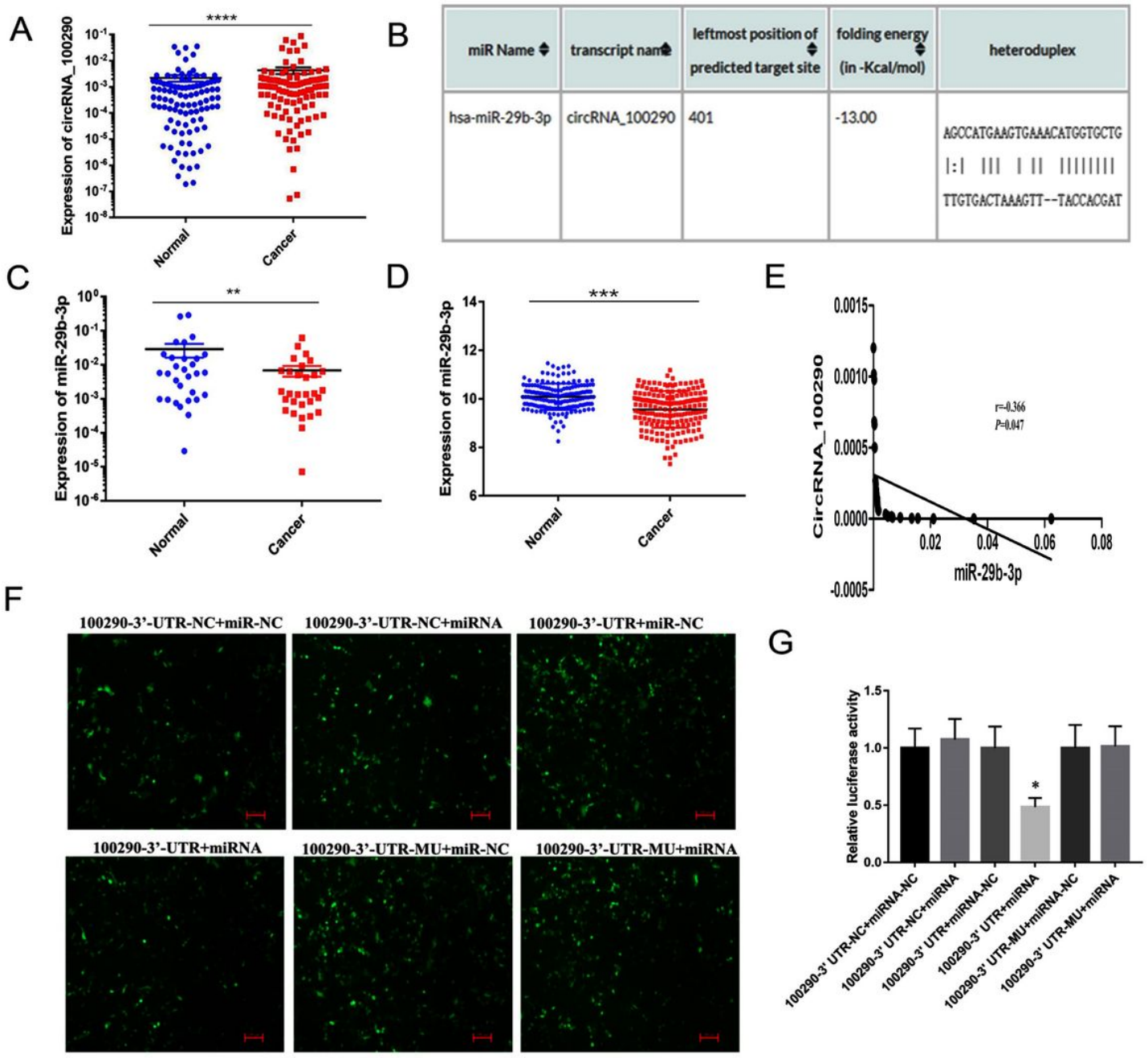

Figure 1

The expression pattern and correlation of circRNA_100290 and hsa-miR-29b-3p in human GC. (A) CircRNA_100290 expression in 102 GC and paired normal tissues was detected by qRT-PCR. Data are means ± SEM.****P<0.0001. (B) RNA22 V2.0 was used to predict the interaction between circRNA_100290 and hsa-miR-29b-3p. (C) The expression of miR-29b-3p in 31 GC and matched normal mucosa was evaluated by qRT-PCR. Data are means ± SEM. **P<0.01. (D) Expression analysis of miR-29b-3p in 184 GC tissues and 168 normal tissues was performed according to EBI database. ***P<0.001. (E) Negative correlation between circRNA_100290 and miR-29b-3p expressions was observed by Pearson

correlation analysis. r= -0.366, P=0.047. (F) Evaluation of transfection efficiency of luciferase reporter gene plasmid by fluorescence microscopy. (G) Relative of luciferase activity of each group was calculated. Luciferase activity of the control group was normalized to 1, *P<0.05.

A

name	geneName	position	targetScanSites	picTarSites	RNA22Sites	PITASites	miRandaSites	programNum	CancerNum
hsa-miR-29b-3p	ITGA11	chr15:68595071-68595077[-]	65[1]	65[1]	0[0]	0[0]	0[0]	2	7

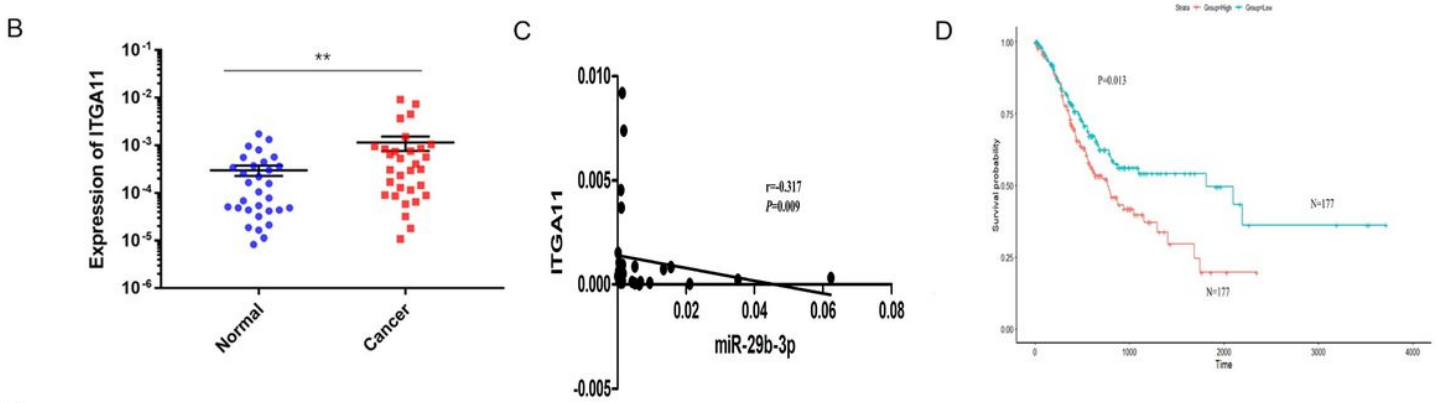

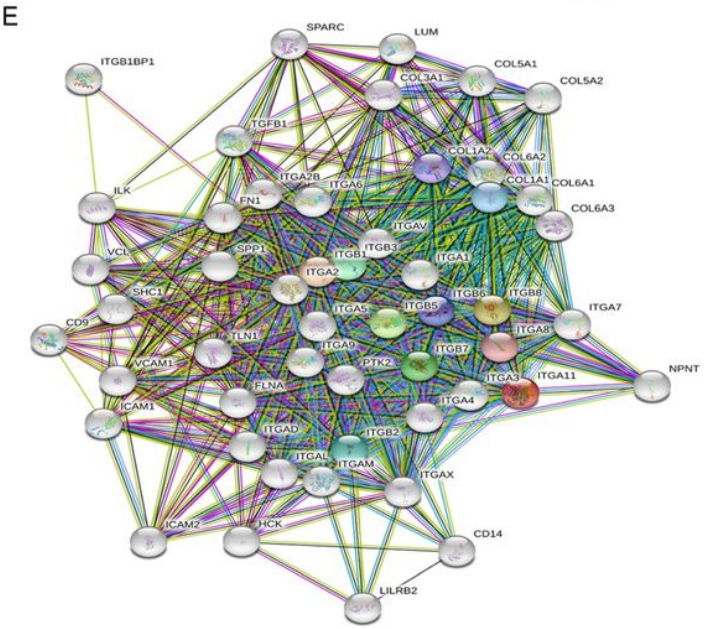

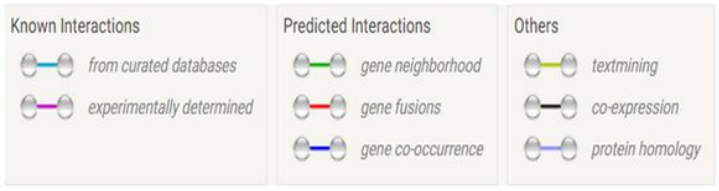

Biological Process (GO)

GO-term	description	count in gene set	false discovery rate
GO:0030198	extracellular matrix organization	41 of 296	8.53e-61
GO:0007229	integrin-mediated signaling pathway	27 of 84	1.03e-45
GO:0007155	cell adhesion	41 of 843	1.18e-43
GO:0007160	cell-matrix adhesion	24 of 119	4.73e-36
GO:0031589	cell-substrate adhesion	25 of 162	3.59e-35
GO:0007166	cell surface receptor signaling pathway	40 of 2198	5.16e-26
GO:0016477	cell migration	29 of 812	2.07e-24

Figure 2

The correlation of hsa-miR-29b-3p and ITGA11 in human GC. (A) One of the most possible targeted genes of hsa-miR-29b-3p was predicted by Starbase. The result had shown that ITGA11 had binding sites with miR-29b-3p. (B) ITGA11 expression in 31 GC and paired normal tissues was detected by qRT-PCR. **P<0.01. (C) Negative correlation between miR-29b-3p and ITGA11 expressions was observed by Pearson correlation analysis. r= -0.317, P=0.009. (D) Prognostic value of the expression of ITGA11 in 354

patients with GC in the TCGA database. (E) protein–protein interaction analysis and gene ontology analysis of ITGA11 using STRING software.

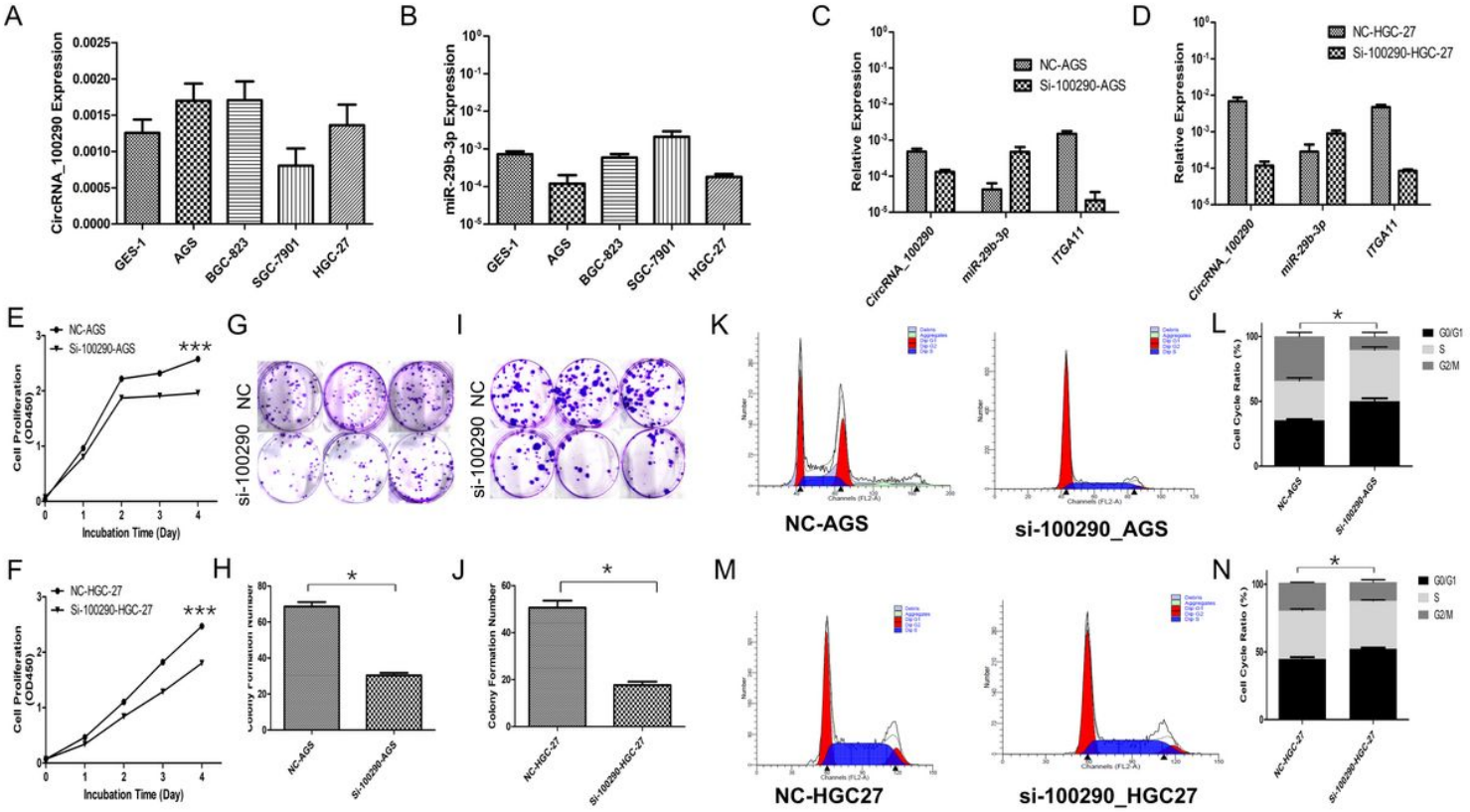

Figure 3

Knocking down circRNA_100290 inhibits GC cell viability, colony-formation and induces G0/G1 cycle arrested. (A) Expressions of circRNA_100290 was detected in four GC cell lines AGS, BGC823, SGC7901, HGC27 and human immortalized normal gastric epithelial cells GES-1 by qRT-PCR assay. (B) Expressions of miR-29b-3p was detected in AGS, BGC823, SGC7901, HGC27 and GES-1 cell lines by qRT-PCR assay. (C) Detection of miR-29b-3p and ITGA11 expression in AGS cell line by qRT-PCR assay after circRNA_100290 siRNA transfection was conducted. (D) Detection of miR-29b-3p and ITGA11 expression in HGC-27 cell line by qRT-PCR assay after circRNA_100290 siRNA transfection was conducted. (E&F) CCK-8 assays were used to evaluate the effects of circRNA_100290 on the proliferation abilities of AGS and HGC27 cells. Knocking-down circRNA_100290 expression significantly inhibited GC cells viability. ***P<0.001. (G&I) Colony formation assays were performed to evaluate the effects of circRNA_100290 on colony-formation abilities of AGS and HGC27 cells. (H&J) The statistical graphs showed that decreasing circRNA_100290 expression suppressed the AGS and HGC27 cells colony-formation ability (*P<0.05). (K&M) The flow cytometry was used to analyze the effects of circRNA_100290 on AGS and HGC27 cell cycle. (L&N) The statistical graphs demonstrated that decreasing circRNA_100290 expression increased the percentage of G0/G1 phase in AGS and HGC27 cells compared with NC control groups(*P<0.05).

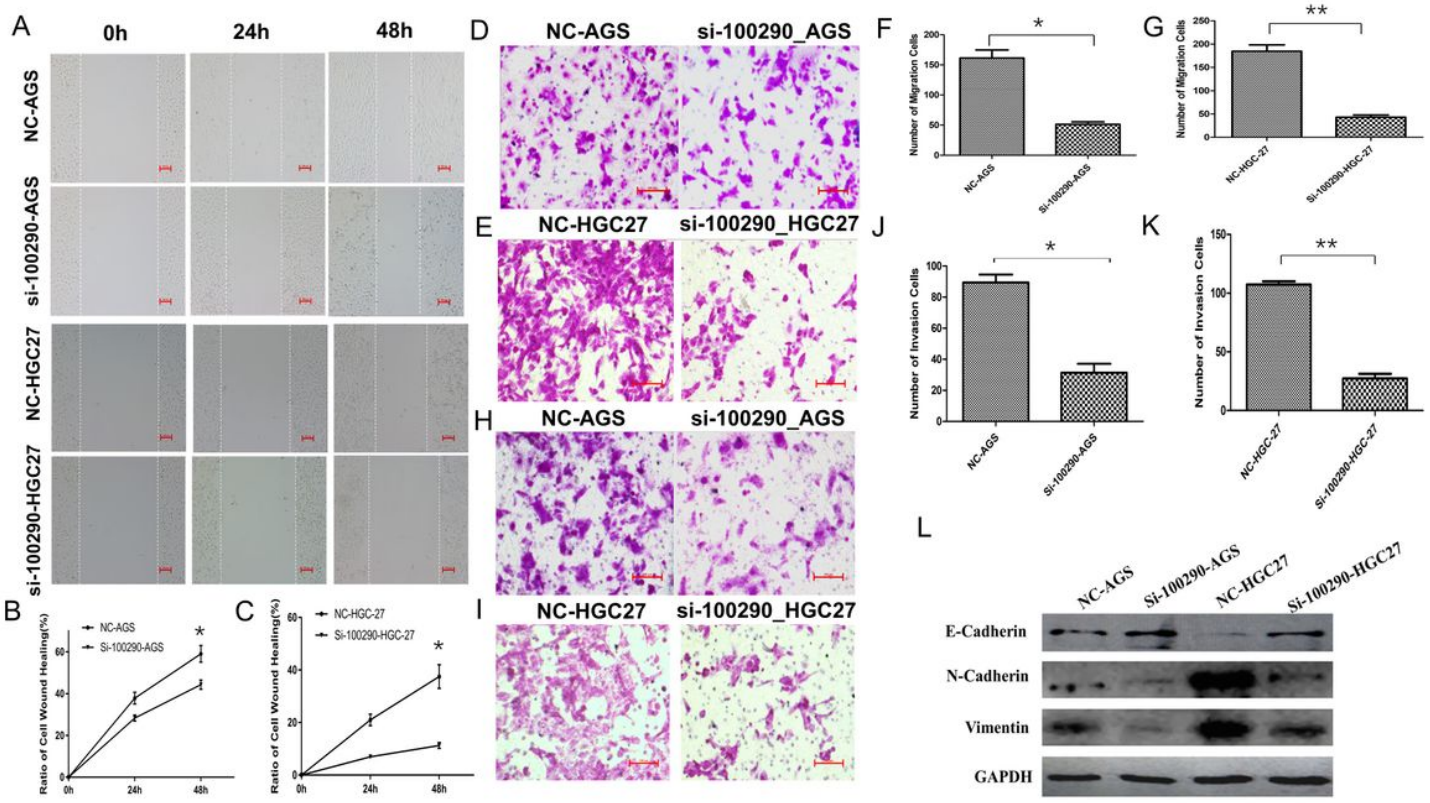

Figure 4

Decreased circRNA_100290 expression suppresses GC cell migration and invasion ability and impedes EMT. (A) Wound-healing assay was performed to evaluate the effects of circRNA_100290 on migration abilities of AGS and HGC27 cells at 0h, 24h, 48h. (B&C) The statistical graphs showed that knocking-down circRNA_100290 obviously inhibited AGS and HGC27 cell wound healing (*P<0.05). (D&E) Transwell migration assay was performed to evaluate the effects of circRNA_100290 on migration abilities of AGS and HGC27 cells. (F&G) The statistical graphs showed that decreased circRNA_100290 expression induced the less AGS and HGC27 cells migrated into lower chamber compared with control groups (*P<0.05, ** P<0.01). (H&I) Transwell invasion assay was performed to evaluate the effects of circRNA_100290 on invasion abilities of AGS and HGC27 cells. (J&K) The statistical graphs displayed that reduced circRNA_100290 expression mediated less AGS and HGC27 cells invaded into lower chamber compared with control groups (*P<0.05, ** P<0.01). (L) Western blot assay was preformed to evaluate the expression of EMT-related proteins including E-cadherin, N-cadherin and Vimentin.

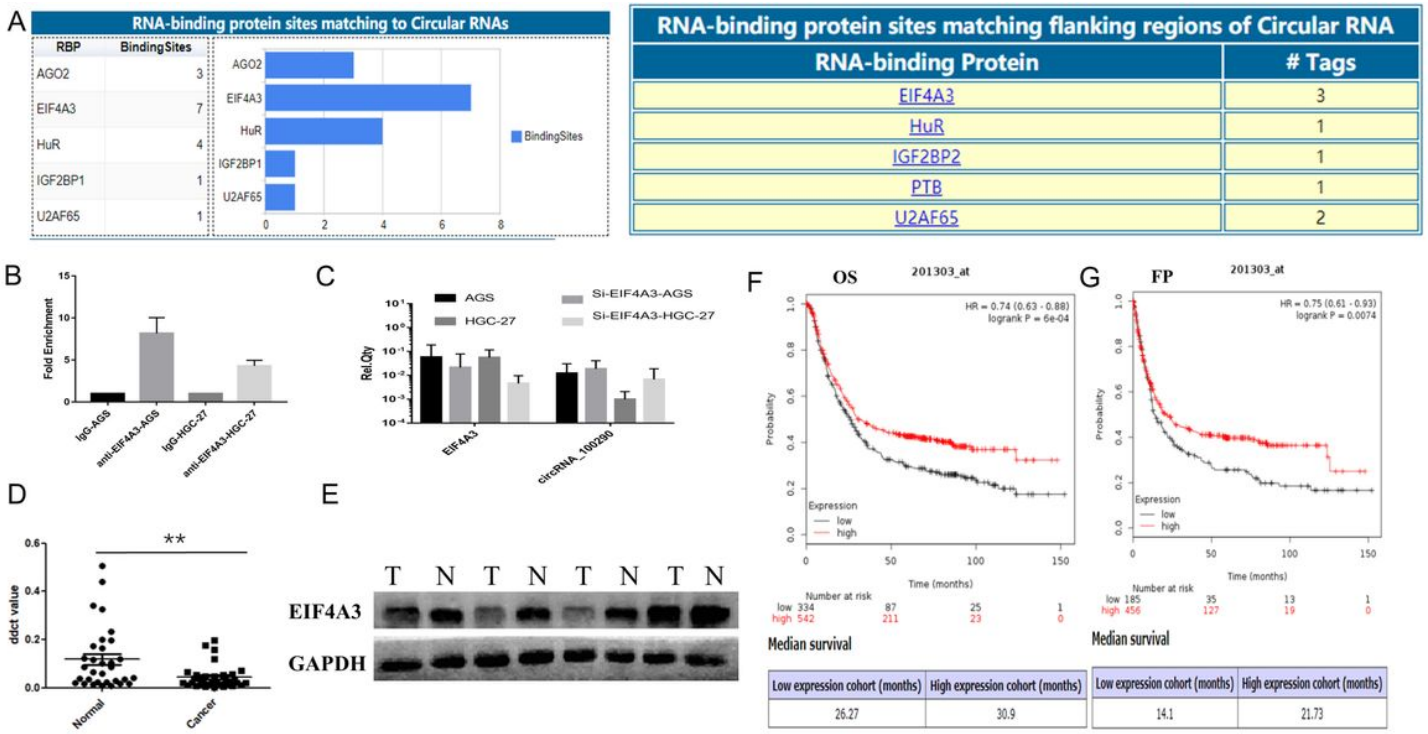

RNA-binding protein sites matching flanking regions of Circular RNA	
RNA-binding Protein	**# Tags**
EIF4A3	3
HuR	1
IGF2BP2	1
PTB	1
U2AF65	2

Figure 5

Study of transcription regulation of EIF4A3 on circRNA_100290. (A) Prediction of circRNA_100290 related RBPs by using Circinteractome software. (B) RIP assay was performed to determine fold enrichment of flanking region of circRNA_100290 by EIF4A3. (C) Detection of circRNA_100290 by qRT-PCR after knocking down of EIF4A3 in AGS and HGC-27 cells. (D) Detection of EIF4A3 expression in 31 GC tissues and paired normal tissues was conducted by qRT-PCR assay. Decreased expression of EIF4A3 was observed in GC tissues. Data are means ± SEM. ** P<0.01. (E) Western blot assay was performed to determine EIF4A3 expression in 31 GC tissues and paired normal tissues. (F&G) Prognosis analysis about OS and FP of ITGA11 in GC patients from the Kaplan–Meier plotter website.